High frequency guided wave defect imaging in monocrystalline silicon wafers

Mathieu Simon, Bernard Masserey, Jean-Luc Robyr, Paul Fromme

Mathieu Simon, Bernard Masserey, Jean-Luc Robyr, Paul Fromme, "High frequency guided wave defect imaging in monocrystalline silicon wafers ," Proc. SPIE 10972, Health Monitoring of Structural and Biological Systems XIII, 1097206 (1 April 2019); doi: 10.1117/12.2513675

SPIE.

Event: SPIE Smart Structures + Nondestructive Evaluation, 2019, Denver, Colorado, United States

High frequency guided wave defect imaging in monocrystalline silicon wafers

Mathieu Simon [a], Bernard Masserey [a], Jean-Luc Robyr [a], and Paul Fromme [b]

[a] Department of Mechanical Engineering, HES-SO University of Applied Sciences and Arts Western Switzerland, Fribourg, Switzerland

[b] Department of Mechanical Engineering, University College London, UK

ABSTRACT

Micro-cracks can be induced in thin monocrystalline silicon wafers during the manufacture of solar panels. High frequency guided waves allow for the monitoring of wafers and characterization of defects. Selective excitation of the first anti-symmetric A_0 guided wave mode was achieved experimentally using a custom-made wedge transducer. The Lamb wave scattered field in the vicinity of artificial defects was measured using a noncontact laser interferometer. The surface extent of the shallow defects varying in size from 30 μm to 100 μm was characterized using an optical microscope. The characteristics of the scattered wave field were correlated to the defect size and the detection sensitivity was discussed.

Keywords: Monocrystalline Silicon, Lamb Waves, Scattering, Ultrasonics

1. INTRODUCTION

In the photovoltaic industry solar panels with high conversion efficiency are manufactured using monocrystalline silicon wafers. Micro-cracks on the surface of the thin and fragile wafers can be induced by the wafer cutting. Increased conversion efficiency and lower manufacturing costs require thin wafers. However, the minimum wafer thickness is in practice limited by the wafer breakage rates [1]. Different techniques have been developed for non-destructive defect detection in silicon wafers, e.g. optical transmission and interferometry, electro- and photo-luminescence imaging, thermography, impact testing, and ultrasonic wave propagation [2, 3]. Guided ultrasonic waves (GUW) [4, 5] can achieve long propagation distances in thin structures and thus provide the required area coverage for in-process monitoring of silicon wafers during manufacture. For composite plates and silicon wafers GUW (S_0 and SH modes) propagation was measured and arrival time and amplitude variation with propagation direction quantified [6]. The propagation of GUW in anisotropic, composite plates has been investigated [7], quantifying energy concentration along the fiber directions [8], modal focusing [9], and defect scattering [10].

For metallic structures, the detection and localization of defects has been demonstrated [11]. Hidden damage [12, 13] and fatigue crack [14-17] detection using high frequency GUW was studied. Experimental measurements of the fundamental Lamb wave modes using laser interferometry allowed crack detection in silicon wafers [18]. Lamb wave amplitude drop in a B-scan configuration was measured using air-coupled transducers for the detection of cracks in monocrystalline and polycrystalline silicon wafers [19]. The scattered GUW pattern (and thus detection sensitivity) for elongated defects like cracks depends on the crack orientation relative to the incident wave field [20, 21]. The scattering of the fundamental A_0 mode [22] and S_0 mode [23] was investigated experimentally and using simulations for defects in plates. For monocrystalline silicon wafers, the ultrasonic wave propagation is direction dependent due to the material anisotropy. Ultrasonic wave energy focusing due to anisotropy was predicted from theory and measured experimentally [24, 25], allowing material properties to be obtained from an inversion of experimental data [26]. The influence of the crystallographic orientation on zero group velocity, cut-off frequency, and amplitude was measured using a line laser source [27]. Guided wave beam skew and phase slowness of the fundamental Lamb modes (A_0 and S_0) in monocrystalline silicon wafers were measured experimentally and compared to theoretical and Finite Element (FE) simulation predictions [28, 29]. Significant guided wave skewing and widening due to the anisotropy was observed [29].

Health Monitoring of Structural and Biological Systems XIII, edited by Paul Fromme, Zhongqing Su, Proc. of SPIE Vol. 10972, 1097206 · © 2019 SPIE
CCC code: 0277-786X/19/$18 · doi: 10.1117/12.2513675

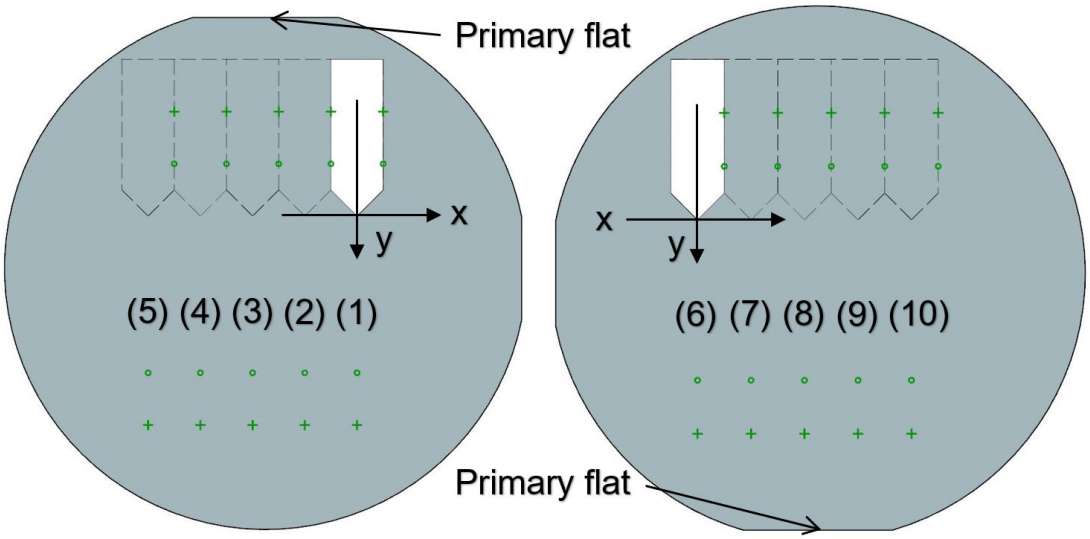

Fig. 1: Schematic of silicon wafer with defect (circles) and wedge transducer (white rectangle) positions marked; surface-printed crosses behind each indent location for localization of defect for measurements.

In this contribution, the near-field scattering of the fundamental A_0 guided wave mode at artificial defects in thin monocrystalline silicon wafers was measured and evaluated. Micro-defects of increasing severity were created using an indenter with different forces and their surface extent characterized from optical microscope images [30]. The first anti-symmetric A_0 Lamb wave mode was selectively excited using a custom-made wedge transducer and measured using a non-contact laser interferometer.

2. EXPERIMENTS

The monocrystalline silicon wafers were boron doped and had <100> crystallographic orientation, 100 mm diameter and 380 µm nominal thickness (Fig. 1). Defects were made using a Vickers indenter with specified force (1 N, 2 N, 3 N, 4 N) and controlled speed. This generated an indent of controlled size, with cracks at the four corners along the <110> direction as shown in Fig. 2 (left). For the higher forces, chipping of the silicon wafer was observed (Fig. 2 right). Defects with chipping of the silicon were not further investigated. 3 indents without significant chipping at each of the 4 force levels were selected for the ultrasonic measurements and evaluation. The indent and overall defect size were evaluated from optical microscopy images. Good correlation between defect size and indent force was found (Fig. 3) with only limited variation.

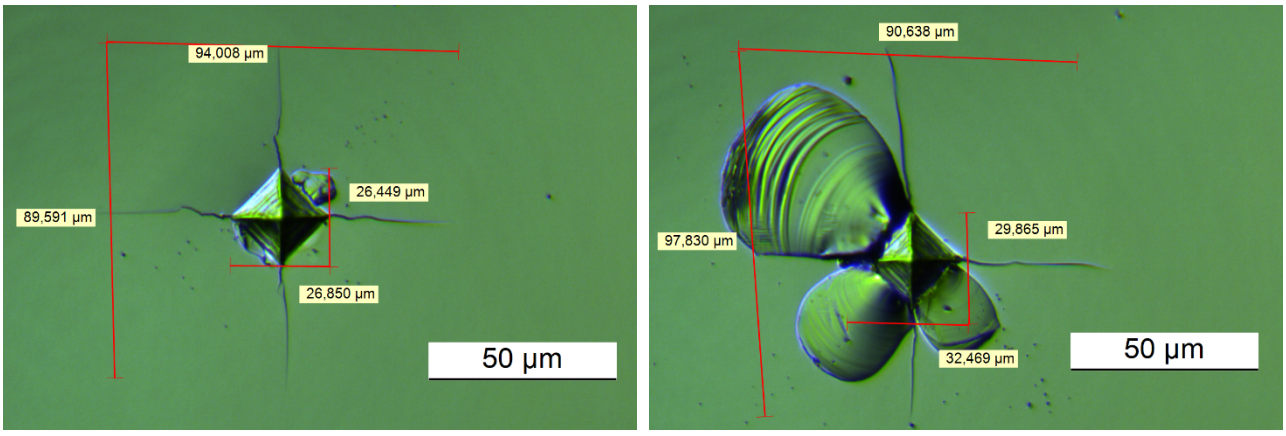

Fig. 2: Microscopy images of defects (indent and surface cracks) with measurements; left: indent with cracks; right: indent with cracks and chipping.

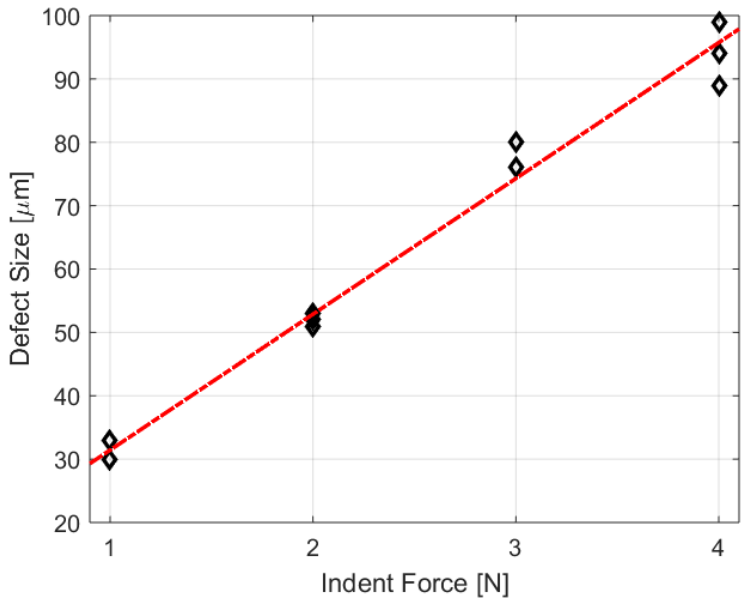

Fig. 3: Correlation of optically measured defect surface extent (indent and surface cracks) with indent force; 3 measurements (diamond) at each force level; linear fit (dash-dotted line).

The silicon wafers were held using a custom-made wafer holder (Fig. 4) to minimize the risk of wafer breakage. The first anti-symmetric Lamb wave mode (A_0 mode) was excited selectively using a custom-made nylon wedge (41° angle) and a commercial piezoelectric transducer. The wedge was pressed against the silicon wafer with controlled force and using standard ultrasonic couplant. A narrowband pulse (12 sinusoidal cycles, Hanning window) with a center frequency of 5 MHz was defined using Labview, generated using an arbitrary function generator, amplified using a power amplifier, and applied to the wedge transducer. The surface displacement (out-of-plane) was measured using a non-contact laser interferometer, positioned parallel to the silicon wafer using a scanning rig. The measured signal was filtered (frequency bandpass: 2-8 MHz), averaged (40 averages) and transferred to a PC for evaluation in Matlab. The maximum amplitude of the measured time trace at each point of the measurement grid was evaluated using the Hilbert transform (envelope of time signal). The measurement grid (centered around the defect) was 400 μm by 400 μm with a step size of 5 μm in both directions to accurately capture local variations in the scattered guided ultrasonic wave field. Several steps were required to center the laser measurement on the defect location as described previously [29, 30]. It should be noted that the accuracy of the relative positioning has not been verified independently.

Fig. 4: Silicon wafer on holder with wedge transducer; reflection of laser beam visible.

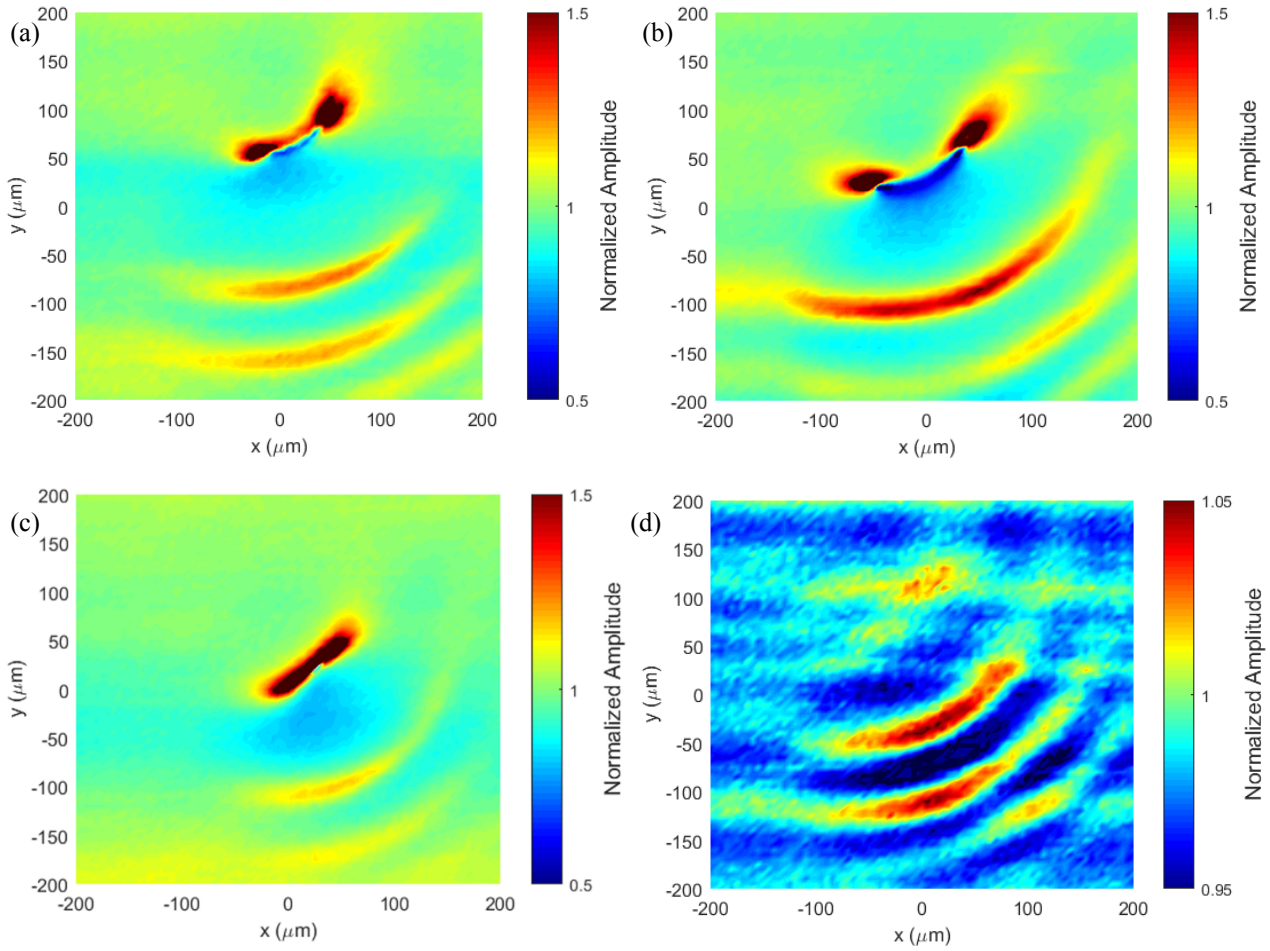

Fig. 5: Measured scattered guided ultrasonic wave field, normalized with incident wave amplitude, A_0 mode at 5 MHz center frequency, step size 5 μm; a) 4 N indent force; b) 3 N indent force; c) 2 N indent force; d) 1 N indent force.

3. SCATTERING AT DEFECTS

Scattered guided ultrasonic wave fields for three defects generated at each indent force were measured, with a representative measurement shown for each force level in Fig. 5. Fig. 6 shows the corresponding optical microscopy images and measurements of surface defect size for the four force levels. From the geometry of the pyramid shaped indenter (opening angle: 136°), for the defect at 4 N force an indent depth of 5 μm was calculated based on the indent size of approximately 27 μm. The cracks from the 4 corners of the indent are aligned along the <110> directions with an overall size of approximately 90-100 μm for the 4 N force defect. The direction of the incident wave propagation is from bottom to top (along y-axis) for the scattered guided ultrasonic wave amplitude field (Fig. 5a). The scattered guided ultrasonic wave field does not show the expected symmetry to the incident wave direction and material anisotropy axes but is skewed towards the right. At the defect location two peaks about 100 μm apart with twice the incident wave amplitude can be seen. Low amplitude can be observed directly in front of the defect. Further away in front of the defect (negative y-axis) an interference pattern with semi-circular areas of high and low amplitude is observed, indicating constructive and destructive interference between the incident wave and the scattered wave.

The scattered guided ultrasonic wave fields for defects due to an indent force of 3 N are reasonably similar (Fig. 5b) to the scattered wave fields for 4 N indent force. From the evaluation of the corresponding microscopy images (Fig. 6b), an overall defect size of approximately 75 μm and an indent depth of 4 μm were obtained. For the indent force of 2 N (Fig. 6c), the overall defect size was measured as about 50 μm and the indent depth was calculated as 3 μm. For the scattered

guided wave fields around these smaller defects, the two amplitude peaks merged to a single peak, with similar high amplitude (Fig. 5c). Similar to the scattered guided ultrasonic wave fields for the larger defects, low amplitude regions and a semi-circular interference pattern were observed. For the indent force of 1 N, the defect size was measured as approximately 30 μm and the depth of the indent as 2 μm (Fig. 6d). Significantly lower maximum amplitude than for the larger defects was observed, with no specific peaks in amplitude (Fig. 5d). Due to the lower amplitude range, the relative noise level of the measurements increased. A clear semi-circular interference pattern could still be seen with similar dimensions to the other scattered fields but lower amplitude.

The maximum amplitude of the scattered guided ultrasonic wave pattern was extracted from the scattered field of the 12 defects (3 each at 4 force levels), normalized with the amplitude of the incident wave for each measurement. Typically, this was one of the amplitude peaks at the defect. Due to the spatial sampling of the scattered wave field with a step size of 5 μm some uncertainty for the magnitude of such a singularity is evident. The maximum amplitude for each defect was plotted against the measured defect size determined from the microscopy images (combined indent and crack length) perpendicular to the propagation direction of the incident wave (Fig. 7). For the smaller defects with a size of up to 55 μm (typically for 1 N or 2 N indent force), the scattered guided ultrasonic wave amplitude is approximately 5-10% of the incident wave amplitude and is observed clearly. For the larger defects a significant increase in scattered wave field amplitude was observed. There is significant variation of the peak scattered guided wave field amplitude with defect size and limited correlation can be seen except for a general increase of peak amplitude with defect size.

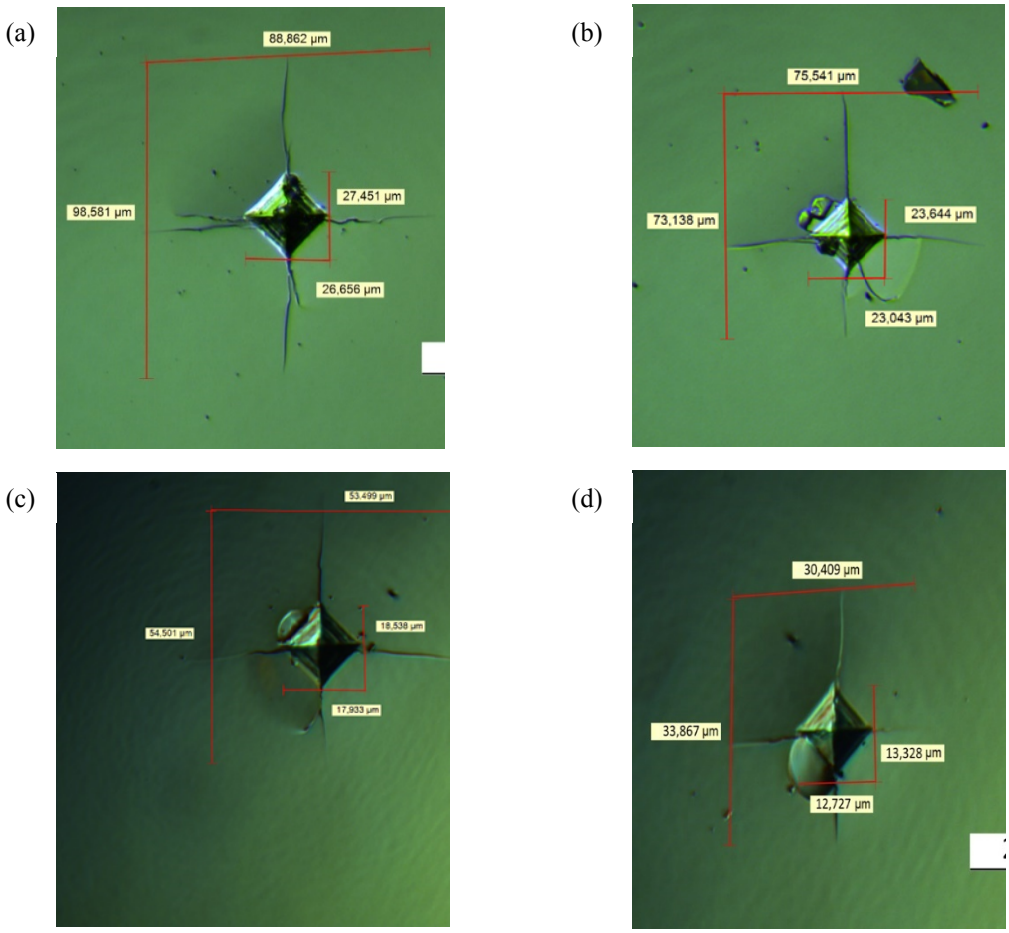

Fig. 6: Optical microscopy image of defect with measurements; a) 4 N indent force; b) 3 N indent force; c) 2 N indent force; d) 1 N indent force.

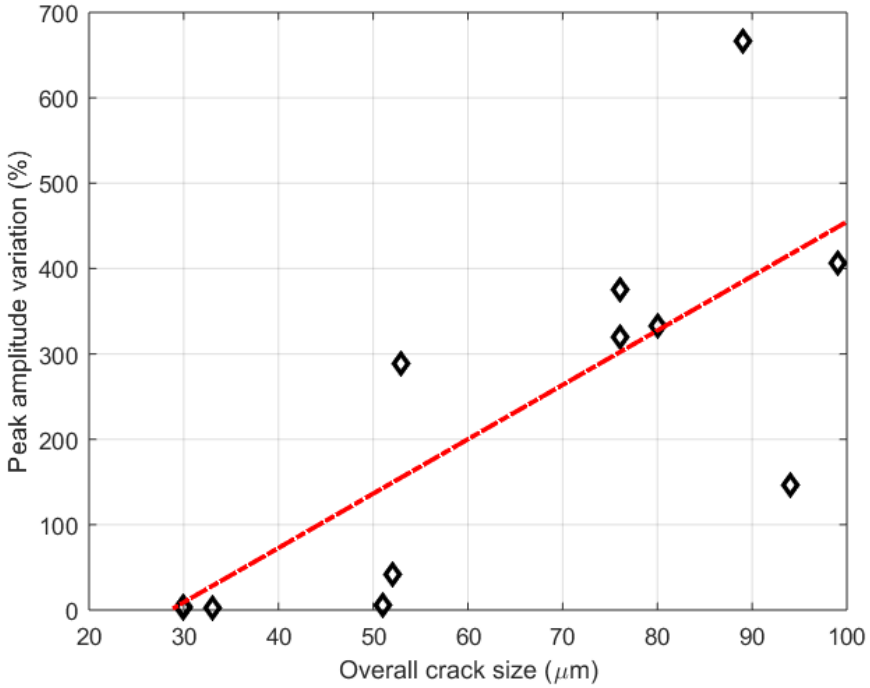

Fig. 7: Percentage of peak amplitude variation (normalized with incident wave amplitude) of measured guided ultrasonic wave scattered plotted against overall defect size (from microscopy image), linear fit (dash-dotted).

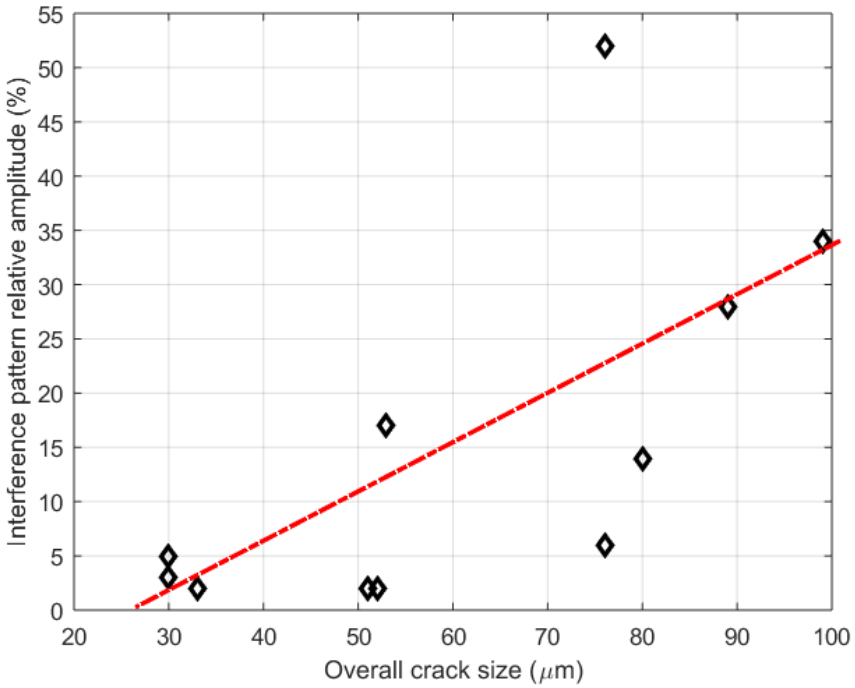

Fig. 8: Percentage of interference amplitude variation (normalized with incident wave amplitude) of measured guided ultrasonic wave scattered plotted against overall defect size (from microscopy image), linear fit (dash-dotted).

There appears to be a significant increase in peak amplitude around 55 μm overall effect size, approximately between a 2N and 3N force indent. The dash-dotted line in Fig. 7 shows the linear fit between peak scattered amplitude (normalized with incident wave amplitude for each defect) and overall defect size.

As the amplitude peaks close to the defect location show a singularity, the amplitude of the scattered wave interference pattern in front of the defect location was quantified and is shown in Fig. 8 against the overall defect size. The scattered guided ultrasonic wave field showed an interference pattern with semi-circular areas of high and low amplitudes for all defects except one, indicative of the constructive and destructive interference between incident and scattered guided wave (Fig. 5). The semicircular patterns were not symmetric to the incident wave direction (y-axis), in line with the overall scattered field amplitude pattern. The innermost semi-circle of high amplitude consistently had a radius of approximately 200 μm, a quarter of the wavelength of the A_0 mode. The amplitude of this pattern should therefore provide an indication of the scattered wave magnitude. Fig. 8 shows the maximum amplitude of this interference pattern against the overall defect size, excluding the peak amplitude at the defect center. A clear increase in amplitude with overall defect size, but again a rather large variation as compared to a linear fit (dash-dotted line) can be seen. The scattered amplitude for the largest defects is about half the amplitude of the incident wave, making it likely that such defects could be detected from a stand-off distance.

4. CONCLUSIONS

The scattering patterns of guided ultrasonic waves at defects of increasing size in silicon wafers were measured and evaluated. Using a custom-made contact wedge transducer, the first anti-symmetric Lamb wave mode (A_0 mode) was excited selectively at a center frequency of 5 MHz in the thin monocrystalline silicon wafers. The scattered guided ultrasonic wave field around artificial defects was measured using a non-contact laser interferometer and the amplitude pattern evaluated. A Vickers hardness testing machine was used to make indents with controlled force. Around the indents, localized micro-cracks originating from the edges of the indent and aligned with the <110> crystallographic direction in the silicon wafer were generated. The defect size on the surface of the silicon wafers was quantified using an optical microscope. Good correlation of the defect size with indent force was found. For higher indent forces, chipping of the silicon wafer was observed for some defects and these were excluded from the ultrasonic measurements.

The guided ultrasonic wave scattered field was measured with high spatial resolution around 3 defects each for 4 different values of the indent force. High peaks of the scattered guided wave amplitude and an approximately semi-circular amplitude interference pattern were observed for all defects. The scattered wave amplitude pattern was consistently not symmetric to the incident wave direction and crystallographic orientation. The scattered wave amplitude increased with defect size, but with significant variation and limited correlation to a linear fit. Further research including the quantification and investigation of the defect depth profile will be required to improve the correlation between defect size and scattered guided wave amplitude. In principle the sensitivity of guided ultrasonic waves for defect detection in monocrystalline silicon wafers was demonstrated.

REFERENCES

[1] Luque, A. and Hegedus, S., [Handbook of Photovoltaic Science and Engineering], Wiley, New York (2011).

[2] Abdelhamid, M., Singh, R. and Omar, M., "Review of microcrack detection techniques for silicon solar cells," IEEE J. Photovoltaics 4, 514-524 (2014).

[3] Israil, M., Ghani, A. and Kerm, Y., "Non-destructive microcracks detection techniques in silicon solar cell," Phys. Sci. Int. J. 4, 1073-1087 (2014).

[4] Rose, J.L., "Standing on the shoulders of giants: An example of guided wave inspection," Mat. Eval. 60, 53-59 (2002).

[5] Fan, Z., Castaings, M., Lowe, M.J.S., Biateau, C. and Fromme, P., "Feature-guided waves for monitoring adhesive shear modulus in bonded stiffeners," NDT&E Int. 54, 96-102 (2013).

[6] Veidt, M. and Sachse, W., "Ultrasonic point-source/point-receiver measurements in thin specimens," J. Acoust. Soc. Am. 96, 2318-2326 (1994).

[7] Murat, B.I.S., Khalili, P. and Fromme, P., "Scattering of guided waves at delaminations in composite plates," J. Acoust. Soc. Am. 139, 3044-3052 (2016).

[8] Leleux, A., Micheau, P. and Castaings, M., "Long range detection of defects in composite plates using Lamb waves generated and detected by ultrasonic phased array probes," J. Nondestruct. Eval. 32, 200-214 (2013).

[9] Chapuis, B., Terrien, N. and Royer, D. "Excitation and focusing of Lamb waves in a multilayered anisotropic plate," J. Acoust. Soc. Am. 127, 198-203 (2010).
[10] Endrizzi, M., Murat, B.I.S., Fromme, P. and Olivo, A., "Edge-illumination X-ray dark-field imaging for visualising defects in composite structures," Compos. Struct. 134, 895-899 (2015).
[11] Hall, J.S., Fromme, P. and Michaels, J.E., "Guided wave damage characterization via minimum variance imaging with a distributed array of ultrasonic sensors," J. Nondestruct. Eval. 33, 299-308 (2014).
[12] Fromme, P., Reymondin, J.-P., and Masserey, B., "High frequency guided waves for disbond detection in multi-layered structures," Acta Acust. united Ac. 103, 932-940 (2017).
[13] Chan, H., Masserey B. and Fromme, P., "High frequency guided ultrasonic waves for hidden fatigue crack growth monitoring in multi-layer model aerospace structures," Smart Mater. Struct. 24, 025037 (2015).
[14] Masserey, B. and Fromme, P., "Analysis of high frequency guided wave scattering at a fastener hole with a view to fatigue crack detection," Ultrasonics 76, 78-86 (2017).
[15] Masserey, B. and Fromme, P., "In-situ monitoring of fatigue crack growth using high frequency guided waves," NDT&E Int. 71, 1-7 (2015).
[16] Masserey, B. and Fromme, P., "In-situ monitoring of fatigue crack growth at fastener holes using Rayleigh-like waves" AIP Conf. Proc. 975, 1484-1491 (2008).
[17] Kostson, E. and Fromme, P., "Fatigue crack growth monitoring in multi-layered structures using guided ultrasonic waves," J. Phys.: Conf. Ser. 195, 012003 (2009).
[18] Song, M.-K. and Jhang, K.-Y., "Crack detection in single-crystalline silicon wafer using laser generated Lamb wave," Adv. Mater. Sci. Eng. 2013, 950791 (2013).
[19] Chakrapani, S.K., Padiyar, M.J. and Balasubramaniam, K., "Crack detection in full size Cz-silicon wafers using lamb wave air coupled ultrasonic testing (LAC-UT)," J. Nondestruct. Eval. 31, 46–55 (2012).
[20] Rouge, C. and Fromme, P., "Directivity of guided ultrasonic wave scattering at notches and cracks," J. Phys.: Conf. Ser. 269, 012018 (2011).
[21] Fromme, P., "Influence of guided ultrasonic wave scattering directionality on the detection sensitivity for SHM of fatigue cracks," Proc. SPIE 7650, 76501M (2010).
[22] Fromme, P. and Sayir, M.B., "Measurement of the scattering of a Lamb wave by a through hole in a plate," J. Acoust. Soc. Am. 111, 1165-1170 (2002).
[23] Diligent, O., Grahn, T., Bostrom, A., Cawley, P. and Lowe, M.J.S., "The low-frequency reflection and scattering of the S0 Lamb wave mode from a circular through-thickness hole in a plate: Finite Element, analytical and experimental studies," J. Acoust. Soc. Am. 112, 2589-2601 (2002).
[24] Maris, H.J., "Enhancement of heat pulses in crystals due to elastic anisotropy," J. Acoust. Soc. Am. 50, 812-818 (1971).
[25] Kim, K.Y., Bretz, K.C., Every, A.G. and Sachse, W. "Ultrasonic imaging of the group velocity surface about the cubic axis in silicon," J. Appl. Phys. 79, 1857-1863 (1996).
[26] Audoin, B., Bescond, C. and Deschamps, M., "Measurement of stiffness coefficients of anisotropic materials from pointlike generation and detection of acoustic waves," J. Appl. Phys. 80, 3760-3771 (1996).
[27] Prada, C., Clorennec, D., Murray, T.W. and Royer, D., "Influence of the anisotropy on zero-group velocity Lamb modes," J. Acoust. Soc. Am. 126, 620-625 (2009).
[28] Fromme, P., Pizzolato, M., Robyr, J.-L. and Masserey, B., "Lamb wave propagation in monocrystalline silicon wafers," J. Acoust. Soc. Am. 143, 287-295 (2018).
[29] Pizzolato, M., Masserey, B., Robyr, J.-L., and Fromme, P., "Guided ultrasonic wave beam skew in silicon wafers," AIP Conf. Proc. 1949, 090005 (2018).
[30] Lauper, M., Fromme, P., Robyr, J.-L., and Masserey, B., "Silicon wafer defect detection using high frequency guided waves," Proc. SPIE 10600, 106000G (2018).